Research Article

Journal of Environmental Nanotechnology

Exceptional Cyclic Stability and Performance Characteristics of a Nanostructured rGO–CNT-WO_3 Supercapacitor Electrode

M. Kalaivani[1], B. Gnanavel[1*] and S. Krithika[2]

[1]PG and Research Department of Physics, Chikkaiah Naicker College, Erode, TN, India
[2]Department of Physical Science, Dr. G. R. Damodaran College of Education, Coimbatore, TN, India
Received: 28.06.2024 Accepted: 12.08.2024 Published: 30.12.2024
*gnanavelphd@gmail.com

ABSTRACT

This study investigated the WO_3-rGO hybrid, a material with great potential as a supercapacitor electrode. This material was produced using a straightforward one-pot hydrothermal synthesis process. A range of analytical techniques including X-ray diffraction, Raman spectroscopy, field emission scanning electron microscopy, transmission electron microscopy,X-ray photoelectron spectroscopy, and Brunauer-Emmett-Teller analysis were used to investigate the structural, morphological, compositional, and surface properties of the prepared materials. The improvement in electrochemical supercapacitive qualities was assessed by comparing pure hexagonal phased WO_3 with different hybrids, which varied based on the concentration of rGO added to it. This evaluation was conducted using cyclic voltammetry, galvanostatic charge/discharge, and electrochemical impedance spectroscopy. The WO_3@rGO(1:5) composite demonstrated a significant increase in capacitance value, reaching 948 F/g. This surpassed the individual capacitance values of rGO (71.11 F/g) and WO_3 (94.22 F/g) at a current density of 4 A/g. Furthermore, the WO_3@rGO(1:5) composite exhibited excellent cycling stability, maintaining 95% of its initial capacitance across 10000 cycles, indicating a promising rate capability and good cycling stability performance.

Keywords: Tungsten oxide; Reduced graphene oxide; Carbon nanotube; Supercapacitor.

1. INTRODUCTION

The increasing economic growth has led to a variety of critical global issues, such as the need for sustainable and environmentally friendly energy sources. Over the past 20 years, significant progress has been made in the development of advanced energy storage and conversion devices, such as ultracapacitors. These devices have emerged as a superior power option due to their impressive features, including high power capacity, fast charging and discharging capabilities, and long-term stability during repeated use. The technology of electrochemical double-layer capacitors is limited by the poor energy density resulting from ion adsorption during charge storage (Abdollahi *et al.* 2019; Bhattacharya *et al.* 2020; Bissett *et al.* 2015; Chen *et al.* 2011; Cheng *et al.* 2015). These capacitors primarily use carbon-based material for electrode fabrication. Pseudocapacitive electrodes, such as those made from transition metal oxides (RuO_2, NiO, MnO_2, SnO_2, Co_3O_4, V_2O_5, MoO_3, IrO_2, etc.) and conductive polymers (polyaniline, polypyrrole, etc.), offer the potential for higher specific capacitance and energy density. This is because charge storage occurs through surface redox faradic reactions. Nevertheless, the combination of the aforementioned electrodes leads to an asymmetrical, battery-like, and composite hybrid capacitor that demonstrates exceptional cycle stability, power output, and specific capacitance. Lately, there has been a growing interest in using nanostructured 2D materials such as carbonaceous graphene, reduced graphene oxides (rGO), metal oxides, metal chalcogenides, and their composites as excellent materials for high-performance supercapacitor electrodes. Tungsten oxide (WO_3) is a stable wide band gap n-type semiconductor with anionic vacancies. It has a hexagonal structure with the space group P6/mmm (Duong *et al.* 2014; Dong *et al.* 2016; Choudhary *et al.* 2016; Cherusseri *et al.* 2019; Du *et al.* 2020).

The various intriguing features of tungsten, such as its ability to have multiple oxidation states, electrochromic properties, high packing density, high energy density, and large pseudocapacitance, have resulted in its extensive use in a wide range of applications. These applications include lithium-ion batteries, gas sensing, photocatalysis, solar cells, electrocatalysis, and electrochromic devices. Lately, there has been a growing focus on transition metal oxides, including Fe_2O_3, TiO_2, MnO_2, ZnO, V_2O_5, and WO_3, as very effective options for portable and flexible supercapacitor electrode materials. WO_3 has received much focus as a suitable electrode material for pseudocapacitors because of its exceptional electrochemical characteristics. WO_3 has notable

characteristics, including a high intrinsic density exceeding 7 gcm^{-3}, a theoretical capacity of around 700 mAh/g, a high energy density, commendable cycling stability, and exceptional rate performance. Gao et al. (year) successfully synthesized tungsten trioxide nanowires on a carbon cloth substrate. These nanowires possess excellent flexibility and demonstrate a high specific capacitance of 521 F/g at an applied current density of 1 A/g. (Zhu *et al*. 2016) presented a study where they observed the formation of hexagonal-phase WO_3 nanopillars on the electrode surface. These nanopillars showed a significant capacitance of up to 421.8 F/g when subjected to a current density of 0.5 A/g. (Wu *et al.* 2016) produced bundles of WO_3 nanotubes using a surfactant-free hydrothermal technique. The resulting asymmetric supercapacitor exhibited a high energy density and long cycling stability, lasting up to 10000 cycles (Li and Kaner 2008; Li *et al.* 2013; Javed *et al.* 2015; Ke and Wang 2016; Ibrahim *et al.* 2016; Ge *et al.* 2017; Han *et al.* 2018; Kumar *et al.* 2018; Varma *et al.* 2018; Jun *et al.* 2019) .

Nevertheless, to address the limitations (such as inadequate electrical conductivity, unstable cyclic performance, and significant irreversible capacity) of WO_3, it is necessary to combine it with a carbonaceous material that exhibits high conductivity, such as carbon nanotubes (CNTs), graphene, or reduced graphene oxide. The enhanced characteristics of the hybrid are attributed to the notable synergistic interaction between the carbon material and metal oxide components. The features of reduced graphene oxide include a large surface area, (which prevents particles from clumping together), excellent chemical functionality and compatibility. The latter property allows for high capacity and conductivity. An investigation on the comparative supercapacitive properties of WO_3/WO_3 was conducted by Yun et al. (Liu *et al.* 2017) who examined the combination of H_2O mixed electrode with graphene nanosheets/WO_3. The graphene nanosheets/WO_3 demonstrated a significantly enhanced specific capacitance of around 143.6 F/g when subjected to a current density of 0.1 A/g. (Xiao-hui *et al.* 2018) synthesized a range of WO_3 nanorods/rGO composites using an in situ electrostatic absorptive hydrothermal technique. These composites exhibited a specific capacitance of 343 F/g at an applied current density of 0.2 A/g. (Fan *et al.* 2019) utilized the ϒ-irradiation technique to fabricate electrodes made of $WO_3 \cdot 2H_2O$/bamboo charcoal. The material had a higher specific capacitance of 391 F/g at an applied current density of 0.5 A/g, in comparison to bamboo charcoal which had a specific capacitance of 108 F/g (Ping t al. 2013). This performance was observed in a 6 M KOH solution, and the material also showed an 82% retention of its capacitance after undergoing 10,000 cycles. A solid-state asymmetric supercapacitor was constructed using graphene-WO_3 nanowires as the active material. This supercapacitor achieved an energy density of 26.7 Wh/kg at a power density of 6 kW/kg. Remarkably, it retained 25 Wh/kg at the same power density even after undergoing 4000 long cycles in a 0.1 M H_2SO_4 electrolyte. A composite of WO_3-rGO nanoflowers was developed by applying a layer of positively charged WO_3 onto negatively charged GO. This composite was proposed for use in supercapacitors. Furthermore, the literature also mentions the utilization of graphene-WO_3 hybrids made through the hydrothermal approach and WO_3/graphene nanoplates prepared using the microwave method as supercapacitor electrodes. These materials exhibited excellent electrochemical characteristics (Purkait *et al.* 2018; Qiao *et al.* 2015; Ratha and Rout 2013; Sambath *et al.* 2015; Shao *et al.* 2018).

2. EXPERIMENTAL PROCEDURE

2.1 Synthesis of WO_3 by Hydrothermal Method

Hydrothermal Synthesis was used for synthesizing the tungsten oxide nanoparticles. A 0.6 g of sodium tungstate (Sigma Aldrich) was dissolved in 10 mL of distilled water and stirred for 10 minutes at room temperature. Further, 3 M HCl (Sigma Aldrich) was added dropwise to the above solution at a maintained pH value of 7. The obtained solution was transferred to Teflon and heated in the oven at 160℃ for 12 hours. The resultant white precipitate was centrifuged, alternatively washed with ethanol and distilled water and then dried at 80℃ for 6 hours.

2.2 Synthesis of Reduced Graphene Oxide Coated WO_3

To prepare the WO_3@rGO nanocomposites, the rGO with the ratio of 1:1 and 1:3 was mixed with the tungsten oxide. The mixture was stirred and ultra-sonicated for 2 hours and heated in the oven at 160℃for 10 hours. The resultant white precipitate was centrifuged, alternatively washed with ethanol and distilled water and then dried at 80℃ for 6 hours. The prepared samples were further characterized. The schematic representation of the WO_3@rGO nanocomposite preparation is shown in Fig. 1.

2.3 Characterization Techniques

Using a Ni-filter and a Rigaku Ultima IV X-Ray diffractometer, the crystallographic data of the as-prepared samples were examined for Cu Kα radiation (wavelength: λ = 0.1541 nm). The morphology of the samples was examined using a field emission scanning electron microscope (FESEM, JEOL JSM-7100F, JEOL Ltd., Singapore) with a maximum operational accelerating voltage of 30 kV. The X-ray photoelectron measurements were taken at VG Microtech, England (Multi Lab, ESCA-3000, sr. no. 8546/1) using Al Kα as the X-ray source and an ultrahigh vacuum. The TEM, JOEL-2100, was used to study transmission electron

microscopy at an acceleration voltage of 200 kV. The electrochemical efficiency of the electrodes was assessed using a PG262A potentiostat/galvanostat (Technoscience Ltd., Bangalore).

Fig. 1: Schematic representation of WO_3@rGO preparation by hydrothermal method

2.4 Electrode Preparation

To do electrochemical measurements, the electrodes were constructed with one milligram of each sample. Ethanol was then used to scatter the material for a period of 15minutes. Drop by drop the resultant slurry was cast over the Ni foam substrate that had been cleaned earlier, which had an area of approximately 0.5 cm^2. Coated foam samples were dried in a vacuum oven for 1 hour at a temperature of 40°C. A hydraulic press with a pressure of 5 tons was used to compress the substrates after they had been cleaned and dried. The flattened samples that were produced were utilized as the working electrodes for the electrochemical apparatus.

3. RESULTS AND DISCUSSION

Fig. 2 display the XRD patterns of pure WO_3 and WO_3-rGO composite crystalline samples. The diffraction signal attributed to graphene oxide (GO) is not detected in any of the composite samples containing tungsten trioxide-reduced graphene oxide (WO_3-rGO). This indicates that GO has been completely reduced during the solvothermal process and that the amount of GO in the composites is relatively low compared to WO_3.

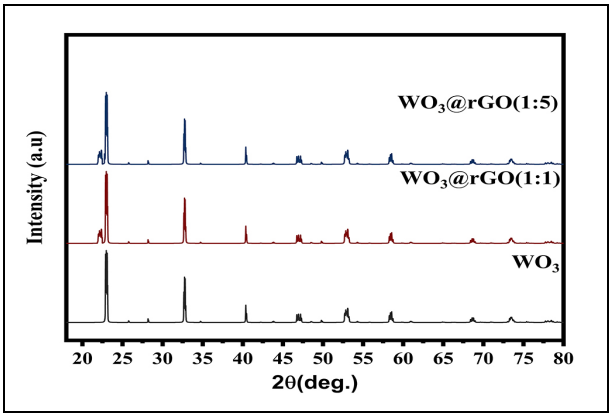

Fig. 2: XRD analysis of WO_3 nanoparticles; WO_3@rGO(1:1); WO_3@rGO(1:5)

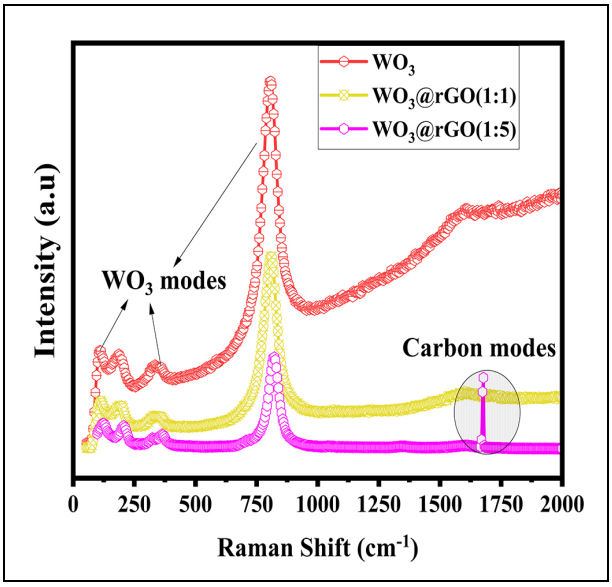

Fig. 3: Raman analysis of (a) WO_3 nanoparticles; WO_3@rGO(1:1); WO_3@rGO(1:5)

The Raman spectra of the WO_3-rGO composites and the pure WO_3 phase are shown in Fig. 3 (a). The lowest wave number peak at around 109 cm^{-1} was mainly caused by the lattice vibrational modes of crystalline WO_3. The vibrations that connect tungsten and oxygen (O-W-O) are seen at higher wavenumbers at ~813 cm^{-1} and ~758 cm^{-1}, as well as at intermediate wavenumbers around ~237 cm^{-1}, ~326 cm^{-1}, and ~667 cm^{-1}, respectively. The presence of characteristic peaks at the highest wave numbers, around 928 cm^{-1} and 936 cm^{-1}, suggests that the oxygen atoms are vibrating in a way that facilitates the development of the symmetric terminal bond W^{6+} = 0.60. Additional intense (as a result of resonant) G (graphite) band at 1602 cm^{-1} is seen in hybrid WO_3-rGO, which is attributed tothe tangential vibration of planar well-configured carbon atoms. Additionally, a diamondoid band at 1354 cm^{-1}, which is the breathing mode of graphitic sp^2-bonded carbon induced by one phonon lattice vibration, was clearly visible, although it was severely disordered (as a result of defects such as edges, surfaces, ripples, etc.). Overloading WO_3 causes the composite peaks to be less intense, and carboxylic groups may cause the D peak to be broader.

Both FESEM and TEM are used to study the morphological characteristics. A distinctive micro-rod-like shape was displayed by the pure WO_3. Fig. 4a shows that the rod- like structures are evenly dispersed and nearly similar in length, ranging from 5 to severaltens of micrometers, with an approximate diameter of around 300 nm. As the concentration of GO increases, the rods transform into little bundles that are both thicker and smaller than before (Fig. 4b, 4c). Better morphological TEM investigation reveals a hexagonal crystal with a conforming selected-area electron diffraction (SAED) pattern, whichis a perfect single crystal (Fig. 4d, 4e inset).

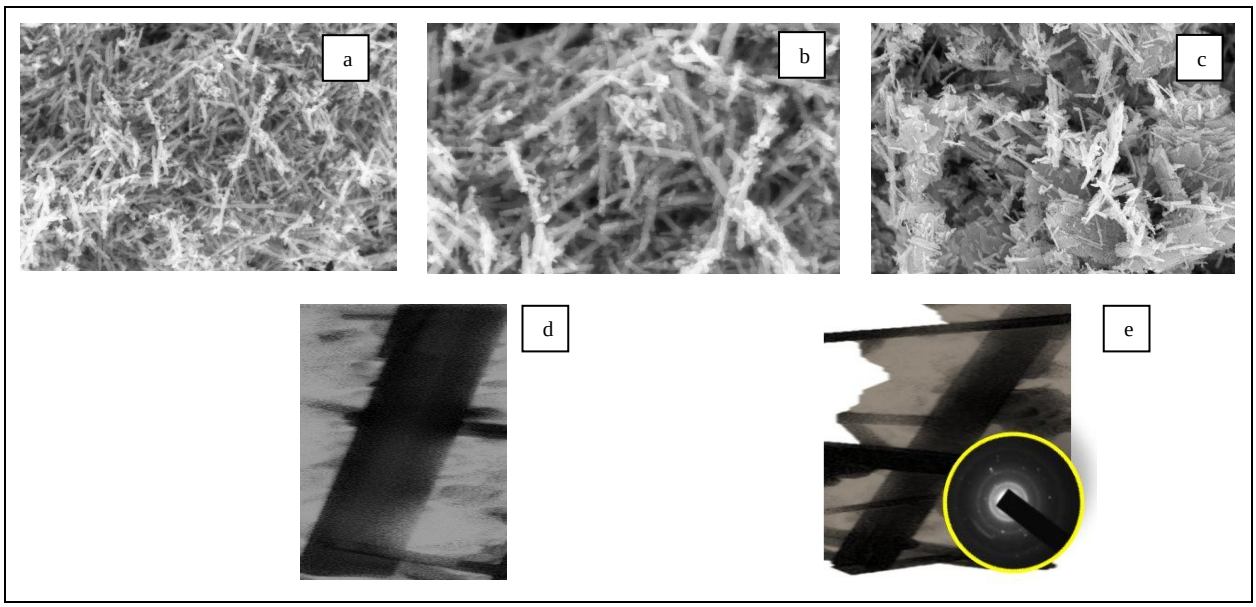

Fig. 4: FESEM and TEM analysis of (a) pure tungsten oxide, (b) WO_3@rGO(1:1), (c)WO_3@rGO(1:5), (d-e) TEM images WO_3@rGO(1:5)

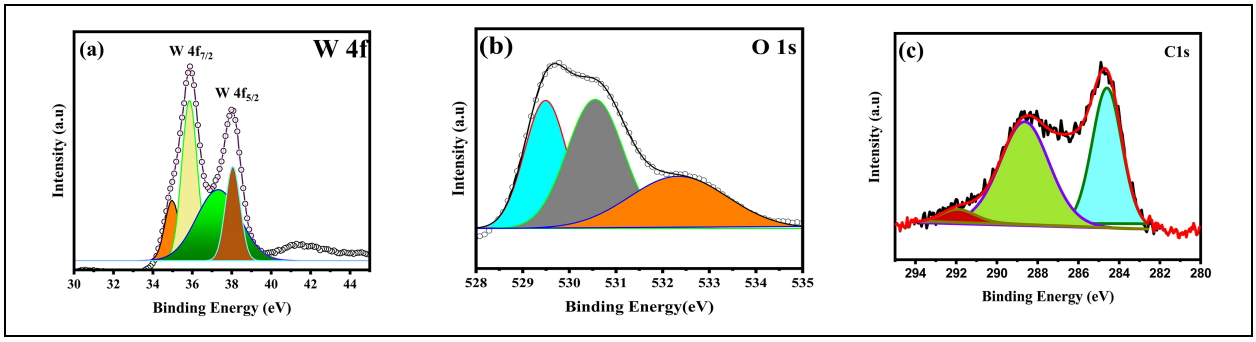

Fig. 5: XPS analysis of WO_3@rGO(1:5) nanocomposites

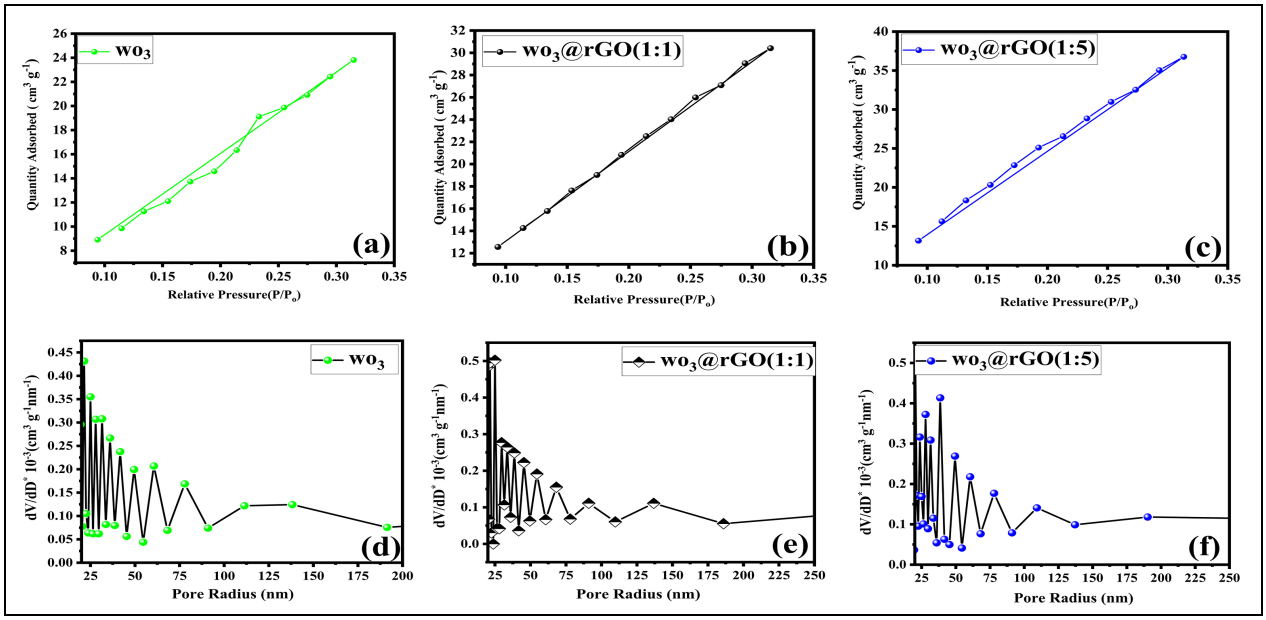

Fig. 6: First row: BET analysis for (a) pure WO_3 (b) WO_3@rGO(1:1) (c) WO_3@rGO(1:5) nanocomposites. Second row: Barrett-Joyner-Halenda plot for (d) pure WO_3 (e) WO_3@rGO(1:1) (f) WO_3@rGO(1:5) nanocomposites

By using X-ray photoelectron spectroscopy (XPS), one can determine the quantitative elemental composition of a material's surface as well as the valence electronic states of elements such as carbon, tungsten, and oxygen. From 0 to 600 eV, the complete survey spectrum of the WO_3-rGO spectra is captured. The XPS doublet peak (Fig. 5a.) of W 4f exhibits two distinct components, namely $W4f_{5/2}$ and $W4f_{7/2}$, with binding energies of 36.1 eV and 38.2 eV, respectively. The measured splitting distance between the two peaks is determined to be 2.1 eV, indicating the presence of W^{6+} oxidation state. Fig. 5b shows that the O1s XPS spectrum of the WO_3-rGO composite is divided into two peaks, one corresponding to the binding energy of 531 eV and the other to the minimum energy required to disassemble W-O and the oxygen anion (O^{2-}) on the Wolfram matrix sites and the hydroxyl groups (-OH) on the composites surfaces. Fig. 5c displays a high-resolution C1s spectrum. The signal with the lowest binding energy at 285.3 eV (C-C, C=C, C-H) indicates the presence of a non-oxygenated sp^2 graphitic carbon-carbon bond on the basal plane of the rGO structure. The additional calibrated peaks located at 286.2 eV and 289.3 eV suggest the presence of residual oxygen-containing functional groups that are particularly bound to carbon atoms, such as carbonyl (-C=O), phenol (-C-OH), and carboxylic (HO-C=O-) (Shen *et al.* 2016; Sun *et al.* 2011).

The Brunauer-Emmett-Teller (BET) study provides information about the surface structural features of the material, including specific surface area, pore size distribution, and N_2 adsorption/desorption isotherm at 77 K. The BET-specific area measurements yielded a specific surface area of 58.3 m^2g^{-1} for WO_3 and 98.667 m^2g^{-1} for WO_3@rGO(1:5). The curve depicted in Fig. 6 (a-c) demonstrates a broad distribution of mesoporous particles, which falls within the category of type IV with the H_3 hysteresis loop (Thripuranthaka *et al.* 2014; Tu *et al.* 2016). The increased porosity structure has a substantial impact on increasing the specific surface area, resulting in a greater number of active sites and thus leading to higher capacitance. Fig. 6(d-f) illustrate the Barrett-Joyner-Halenda (BJH) plot, which displays the average pore diameter ranging from 2 to 33 nm for the generated WO_3 and its rGO composites.

Using a three-electrode electrochemical device that includes Ag/AgCl, platinum wire, and modified Ni foam deposited with the as-prepared sample as the reference, counter, and working electrode, the electrochemical properties of the as-grown pure and WO_3-rGO hybrid samples were evaluated. Cyclic voltammetry (CV), galvanostatic charge- discharge (GCD), and electrochemical impedance spectroscopy (EIS) with a 3M KOH basic electrolyte were used to evaluate the hybrids electrochemical performance gains.

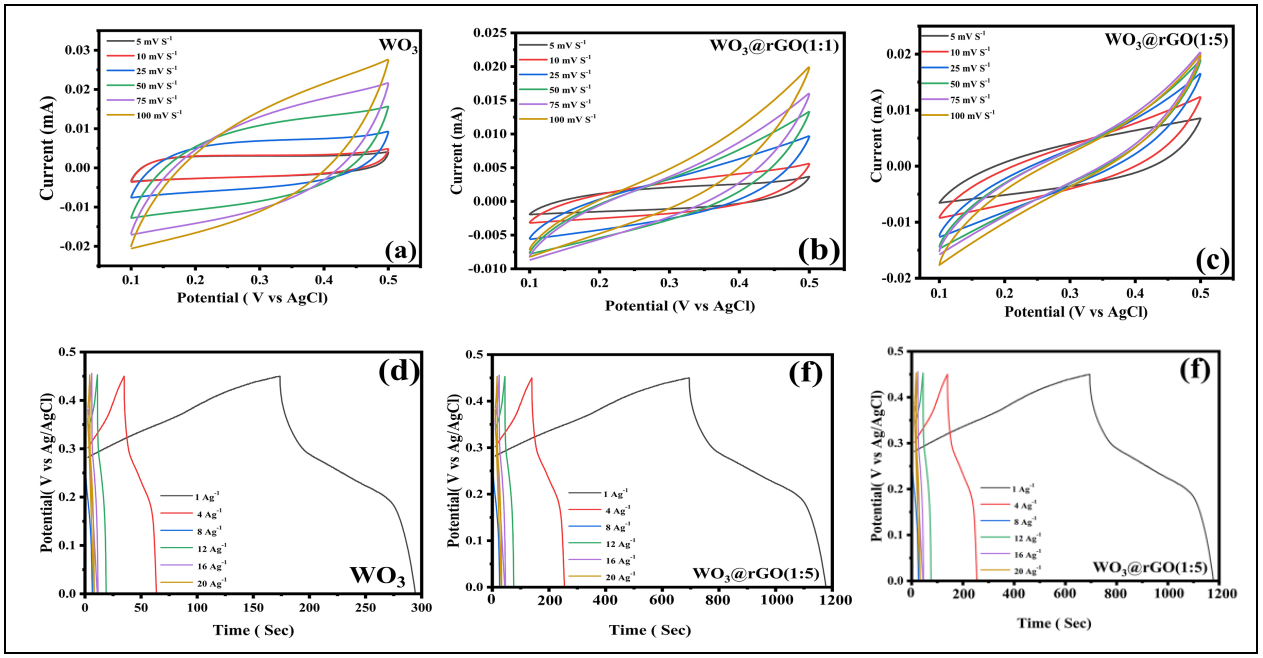

Fig. 7: First row: CV analysis at varying scan rates from 5 mVs^{-1} to 100 mVs^{-1} (a) pure WO_3 (b) WO_3@rGO(1:1) and (c) WO_3@rGO(1:5). Second row: GCD analysis by varying current density for (d) pure WO_3 (e) WO_3@rGO (1:1) and (f) WO_3@rGO(1:5)

Fig. 7(a-c) exhibits the sweep voltammograms of the pristine and hybrid electrodes, obtained at a scan rate of 5 mV/s. The CV curves of WO_3@rGO(1:1) are shown in Fig. 7b. The results indicate that the WO_3@rGO(1:5) electrode demonstrates superior supercapacitor performance, attributed to its elevated electrochemical activity. The rapid current responses observed when charge carriers in WO_3 and rGO rapidly reciprocate and accelerate suggest good reversibility (Xia *et al.* 2015). This corresponds to a reversible reaction

between W^{5+} and W^{6+}. The rise in redox peak current and greater curve area were accompanied by an increase in scan rate, indicating a decrease in the specific capacitance value. The CV curves of WO_3@rGO(1:5) micro-rods were combined at various scan rates (ranging from 5 mV/s to 100 mV/s) within a potential range of 0 to 0.45 V. These curves are shown in Fig. 7c. High reversible redox activity was demonstrated by WO_3@rGO(1:5), resulting in an improved specific capacitance value of 828.45 F/g at a scanning rate of 5 mV/s. In addition, the pseudocapacitive energy storage properties were analyzed using aprecise and dependable galvanostatic charge/discharge approach to further assess the electrochemical properties at various current densities. The specific capacitance ofWO_3@rGO was determined by the discharge process was shown in Fig 7 (d-f). Thus, the incorporation of supplementary rGO content into the pure characteristics of the hybrid material results in improved quick electrical charge transfer pathways, enhanced crystallinity of WO_3, stronger interfacial contacts, and higher electrochemical properties.

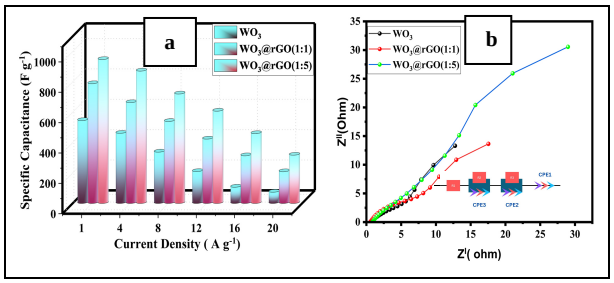

Fig. 8: (a) Specific capacitance of pure WO_3, WO_3@rGO(1:1) and WO_3@rGO(1:5) by varying current density (b) EIS analysis of pure WO_3, WO_3@rGO (1:1) and WO_3@rGO (1:5)

Specific capacitance data of pure WO_3, WO_3@rGO(1:1) and WO_3@rGO(1:5) by varying the current density are represented in Fig. 8a. The values for the curves were as follows: 948 F/g, 872 F/g, 721 F/g, 608 F/g, 460 F/g and 318 F/g. These values correspond to current densities of 1 A/g, 4 A/g, 8 A/g, 12 A/g, 16 A/g, and 20 A/g, respectively. The decrease in specific capacitance with an increase in current density is primarily caused by two factors: the resistance of the electrode and the insufficient faradaic redox reaction of the active material. For a pure sample, the capacitance experiences a significantly faster decline compared to WO_3@rGO(1:5).

A significant level of capacitance retention, reaching 95%, is seen for the WO_3@rGO(1:5) electrode, demonstrating excellent stability even after undergoing 10,000 charge-discharge cycles. The charge-discharge measurements conducted on these materials at high current density ranges demonstrate their rate capacity, which is attributed to the synergistic effect of the 2D nanocomposite. Thus, results demonstrate that the WO_3@rGO(1:5) when used as a supercapacitor electrode has much superior stability, exceptional capacitance, and charge storage capacity compared to the bare electrodes WO_3 and WO_3@rGO(1:1).

The resistive and capacitive characteristics of the electrode were investigated by performing Electrochemical Impedance Spectroscopy (EIS) on both bare and WO_3@rGO(1:5) electrodes.This is done using a three-electrode system, with a frequency range of 0.05 Hz to 100 kHz and an open circuit perturbation potential of 5 mV. The EIS plot often displays two separate types of components: (a) a semicircle located in the higher frequency region, and (b) an apparent straight line observed in the lower frequency zone. The semicircle represents the faradaic reactions, while its diameter indicates the interfacial transfer resistance (R_{ct}). As a result of the slow pace at which charge is transferred in pure samples, the Rs value is consistently higher than that of composite samples (RSP=12.36 Ω > RSWG-80=2.991Ω). Fig. 8b depicts the Nyquist plot for WO_3 and WO_3-rGO using Randle's equivalent circuit, which is shown in the inset. In the Randle's circuit, R_{ct} represents the diffusion resistance, which is composed of three resistance components: (a) the ionic resistance of the liquid electrolyte, (b) the resistance of the active material, and (c) the contact resistance between the current collector (Ni foam) and the active material. The equivalent circuit includes a Faradic impedance linked in parallel with double layer capacitance (C_{dl}). The Faradic impedance is a combination of charge transfer resistance (R_{ct}) and Warburg impedance (W) connected in series. In Fig. 8c, a steep straight line that is nearly vertical to the real axis (WO_3, WO_3@rGO(1:1))) has superior capacitive performance, indicating a lower diffusion resistance compared to the clean sample. For supercapacitors, charge accumulation occurs within the capacitor through either ionic transport or ion intercalation processes. This suggests that the electron conductivity of WO_3@rGO(1:5) increases as the capacitance increases. In the case of WO_3@rGO(1:1), the increased combination of rGO and WO_3 nanorods leads to agglomeration, which reduces the surface area. This reduction hinders charge transfer and ion diffusion compared to WO_3@rGO(1:1) during electrochemical processes, resulting in a decrease in semicircle radii.

3.1 Fabrication of Asymmetric Capacitor

The excellent electrochemical performance exhibited by the electrodes motivated us to fabricate an asymmetric supercapacitor. The asymmetric supercapacitor was constructed byutilizing rGO as the anode and tungsten trioxide/tungsten disulfide (WO_3/WS_2) as the cathode in an aqueous electrolyte containing 6 M KOH. Fig. 9 (a) displays the CV curves of rGO and WO_3/WS_2 electrodes, showcasing their ideal capacitance and steady voltage window of operation when scanned at a rate of 100 mV/s. In order to maintain the steady functioning of the asymmetric device and optimize its capacitance and cycle life, it is crucial to

maintain a charge balance between the cathode and anode according to the following relation (Zhang *et al.* 2011):

$$q^{+} = q_{-}$$

$$C_{+} \times \Delta E_{+} \times A_{+} = C_{-} \times \Delta E_{-} \times A_{-} \quad \ldots (1)$$

Let q^{+} represent the charges stored on the cathode and q^{-} represent the charges stored on the anode. The symbols C, ΔE, and A represent the areal capacitance, potential window, and active electrode area of the corresponding electrodes, respectively. Based on the three-electrode investigations, it is evident that the rGO electrode operates within the range of -0.3 to 0.5 V vs AgCl. The aforementioned information suggests that the asymmetrical supercapacitor cell, when constructed with these two electrodes, can achieve a maximum operational voltage of 1.3 V or higher, contingent upon the overpotential. Additional electrochemical tests were conducted at a voltage of 1.5 V for the asymmetric cell.

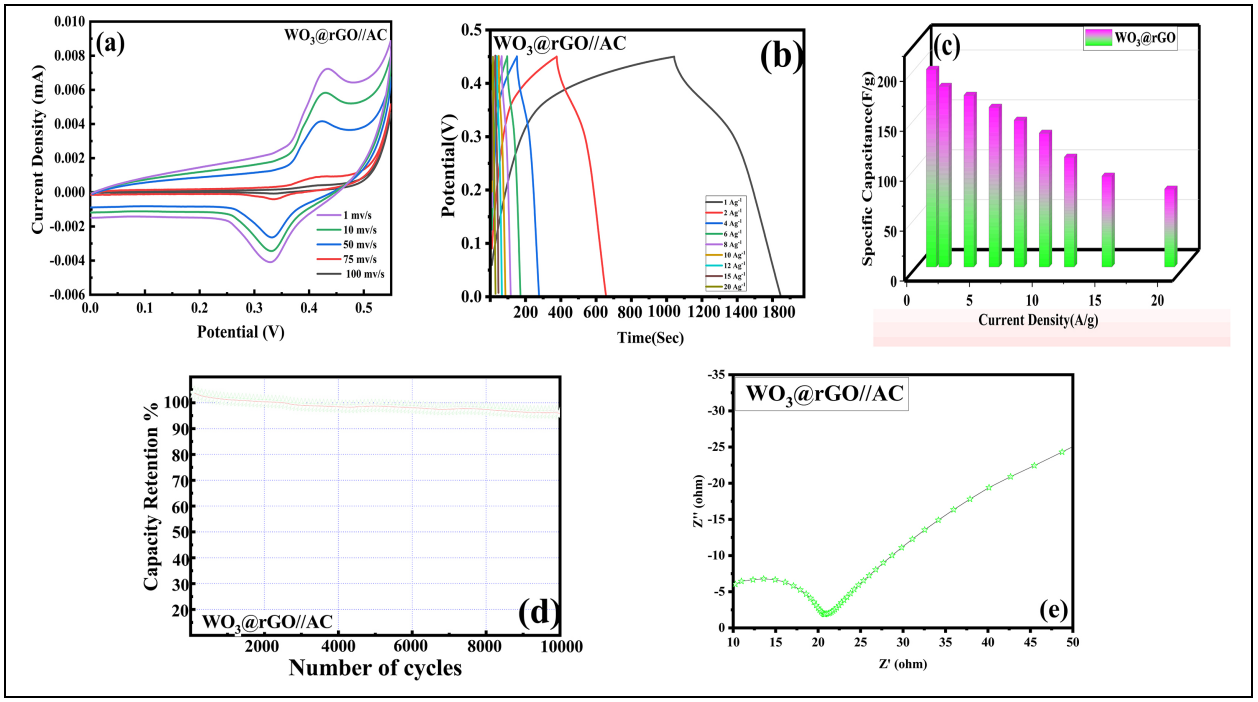

Fig. 9: (a-e) CV, EIS and GCD analysis of WO_3@rGO (1:5)//AC

The rectangular and symmetrical CV curves of the asymmetric cell remained consistent while it was scanned at rates ranging from 5 to 100 mV/s. This indicates that the cell exhibits good capacitance behavior and rate capacity. The GCD patterns of the prepared asymmetric device were recorded for different current densities from 1 Ag^{-1} to 20 Ag^{-1} (Fig 9b). It shows that the capacitance was maintained at high level even at higher current densities with minimal capacity loss. The insertion of rGO on the surface of WO_3 greatly enhances the electron transport between the electrodes and reduces the side reactions that occur at the surface of the electrodes, which greatly enhances the electrochemical performance of the electrodes for long-term cycling. The specific capacitance values from GCD patterns is shown in Fig 9c. The fabricated asymmetric device delivers a capacity retention of about 92% after 10000 cycles (Fig 9d).

The electrical properties of fabricated device electrodes were investigated using electrochemical impedance spectroscopy (EIS). Fig. 9e depicts the impedances of electrodes that were fabricated as-is in a 6 M KOH electrolytic solution. The measurements were taken across a frequency range of 1 Hz to 100 kHz, with an alternating current (AC) amplitude of 10 mV. It is evident that on the real component, specifically the Z0 axis, the size of a semicircle in the high-frequency range is linked to the R_{ct}, suggesting increased ion diffusion into the pores of the electrode. Within the high-frequency range, the Nyquist plot of each electrode exhibits no semicircle, showing the presence of excellent super-capacitive characteristics. The value being 29.40. The WO_3@rGO(1:5)//AC electrode has a much lower charge transfer resistance of 5.182 Ω compared to other electrodes. A vertical curve above 45° in the low-frequency range indicates significant super-capacitive behavior with minimal resistance to diffusion in the electrodes. The circuit with similar characteristics was utilized to examine the impedance spectra generated. The enhanced electrochemical performance can be attributed to the presence of the rGO conductive network, which facilitates quick electron transfer, and the WO_3 nanorods, which promote electrolyte penetration and minimize ion and electron transport paths.

The improved electrochemical performance of WO_3@rGO(1:5)//AC can be ascribed to the existence of tungsten trioxide and rGO nanostructures. These features enhance the surface area of contact between the electrolyte and electrode, hence improving the movement of ions and ultimately resulting in improved rate capability. The results suggest that WO_3@rGO(1:5)//AC is a highly suitable option for energy storage devices with exceptional efficiency. Additionally, the fabricated electrodes have capacitance and cyclic stability that are either comparable to or larger than those of the other electrodes, suggesting their superior electrochemical performance.

4. CONCLUSION

The synthesis of WO_3@rGO demonstrated in this study has revealed the potential to produce a consistent thin film with remarkable electrochemical capacitive properties using a straightforward, cost-effective, and eco-friendly method. Additionally, the approach is easily scalable. The electrochemical findings revealed a synergistic interaction between the two constituents of the mentioned nanocomposite, resulting in enhanced electron mobility, increased surface area, and improved specific capacitance. The synergistic combination of the components significantly enhanced the cyclic stability, resulting in a 2.4-times increase compared to WO_3. Thus, this work presents a method for fabricating a material with precise and stable properties, which shows great potential for use as a supercapacitor.

FUNDING

There is no funding source.

CONFLICT OF INTEREST

The authors declared no conflict of interest in this manuscript regarding publication.

REFERENCES

Abdollahi, A., Abnavi, A., Ghasemi, S., Mohajerzadeh, S. and Sanaee, Z., Flexible free-standing vertically aligned carbon nanotube on activated reduced graphene oxide paper as a high performance lithium ion battery anode and supercapacitor, *Electrochim. Acta.*, 320, 134598(2019). https://doi.org/10.1016/j.electacta.2019.134598

Bhattacharya, G., Fishlock, S. J., Pritam, A., Sinha, R. S. and McLaughlin, J. A., Recycled Red Mud–Decorated Porous 3D Graphene for High-Energy Flexible Micro-Supercapacitor, *Adv. Sustainable Syst.*, 4(4), 1900133(2020). https://doi.org/10.1002/adsu.201900133

Bissett, M. A., Kinloch, I. A. and Dryfe, R. A. W., Characterization of MoS_2 –Graphene Composites for High-Performance Coin Cell Supercapacitors, *Am. Chem. Soc. Appl. Mater. Interfaces*, 7(31), 17388–17398(2015). https://doi.org/10.1021/acsami.5b04672

Chen, Y., Zhang, X., Zhang, D., Yu, P. and Ma, Y., High performance supercapacitors based on reduced graphene oxide in aqueous and ionic liquid electrolytes, *Carbon*, 49(2), 573–580(2011). https://doi.org/10.1016/j.carbon.2010.09.060

Cheng, Z., Wang, Z., Shifa, T. A., Wang, F., Zhan, X., Xu, K., Liu, Q. and He, J., Au plasmonics in a WS2-Au-CuInS2 photocatalyst for significantly enhanced hydrogen generation, *Appl. Phys. Lett.*, 107(22), 223902(2015). https://doi.org/10.1063/1.4937008

Cherusseri, J., Choudhary, N., Sambath, K. K., Jung, Y. and Thomas, J., Recent trends in transitio n metal dichalcogenide based supercapacitor electrodes, *Nanoscale Horiz.*, 4(4), 840–858(2019). https://doi.org/10.1039/C9NH00152B

Choudhary, N., Li, C., Chung, H. S., Moore, J., Thomas, J. and Jung, Y., High-Performance One-Body Core/Shell Nanowire Supercapacitor Enabled by Conformal Growth of Capacitive 2D WS_2 Layers, *Am. Chem. Soc. Nano*, 10(12), 10726–10735(2016). https://doi.org/10.1021/acsnano.6b06111

Dong, L., Xu, C., Li, Y., Huang, Z. H., Kang, F., Yang, Q. H. and Zhao, X., Flexible electrodes and supercapacitors for wearable energy storage: a review by category, *J. Mater. Chem. A.*, 4(13), 4659–4685(2016). https://doi.org/10.1039/C5TA10582J

Du, J., Liu, L., Hu, Z., Yu, Y., Zhang, Y., Hou, S. and Chen, A., Raw-Cotton-Derived N-Doped Carbon Fiber Aerogel as an Efficient Electrode for Electrochemical Capacitors, *Am. Chem. Soc. Sustainable Chem. Eng.*, 6(3), 4008–4015(2018). https://doi.org/10.1021/acssuschemeng.7b04396

Duong, B., Yu, Z., Gangopadhyay, P., Seraphin, S., Peyghambarian, N. and Thomas, J., High Throughput Printing of Nanostructured Carbon Electrodes for Supercapacitors, *Adv. Mater. Inter.*, 1(1), 1300014(2014). https://doi.org/10.1002/admi.201300014

Ge, Y., Jalili, R., Wang, C., Zheng, T., Chao, Y. and Wallace, G. G., A robust free-standing MoS2/poly(3,4ethylenedioxythiophene):poly(styren esulfonate) film for supercapacitor applications, *Electrochim. Acta.*, 235, 348–355(2017). https://doi.org/10.1016/j.electacta.2017.03.069

Han, Y., Ge, Y., Chao, Y., Wang, C. and Wallace, G. G., Recent progress in 2D materials for flexible supercapacitors, *J. Energy Chem.*, 27(1), 57–72(2018). https://doi.org/10.1016/j.jechem.2017.10.033

Ibrahim, I., Lim, H. N., Huang, N. M. and Pandikumar, A., Cadmium Sulphide-Reduced Graphene Oxide-Modified Photoelectrode-Based Photoelectrochemical Sensing Platform for Copper(II) Ions, *Public Lib. Sci. ONE*, 11(5), e0154557(2016). https://doi.org/10.1371/journal.pone.0154557

Varma, J. S., Sambath Kumar, K., Seal, S., Rajaraman, S. and Thomas, J., Fiber-Type Solar Cells, Nanogenerators, Batteries, and Supercapacitors for Wearable Applications, *Adv. Sci.*, 5(9), 1800340(2018). https://doi.org/10.1002/advs.201800340

Javed, M. S., Dai, S., Wang, M., Guo, D., Chen, L., Wang, X., Hu, C. and Xi, Y., High performance solid state flexible supercapacitor based on molybdenum sulfide hierarchical nanospheres, *J. Power Sources*, 28563–69(2015). https://doi.org/10.1016/j.jpowsour.2015.03.079

Jiao, Z., Wang, J., Ke, L., Liu, X., Demir, H. V., Yang, M. F. and Sun, X. W., Electrochromic properties of nanostructured tungsten trioxide (hydrate) films and their applications in a complementary electrochromic device, *Electrochim. Acta.*, 63, 153–160(2012). https://doi.org/10.1016/j.electacta.2011.12.069

Jun, B. M., Kim, S., Heo, J., Park, C. M., Her, N., Jang, M., Huang, Y., Han, J. and Yoon, Y., Review of MXenes as new nanomaterials for energy storage/delivery and selected environmental applications, *Nano Res.*, 12(3), 471–487(2019). https://doi.org/10.1007/s12274-018-2225-3

Ke, Q. and Wang, J., Graphene-based materials for supercapacitor electrodes – A review, *J. Mater.*, 2(1), 37–54(2016). https://doi.org/10.1016/j.jmat.2016.01.001

Kumar, K. S., Choudhary, N., Jung, Y. and Thomas, J., Recent Advances in Two-Dimensional Nanomaterials for Supercapacitor Electrode Applications, *Am. Chem. Soc. Energy Lett.*, 3(2), 482–495(2018). https://doi.org/10.1021/acsenergylett.7b01169

Li, D. and Kaner, R. B., Graphene-Based Materials, *Sci.*, 320(5880), 1170–1171(2008). https://doi.org/10.1126/science.1158180

Li, X., Zhao, T., Chen, Q., Li, P., Wang, K., Zhong, M., Wei, J., Wu, D., Wei, B. and Zhu, H., Flexible all solid-state supercapacitors based on chemical vapor deposition derived graphene fibers, *Phys. Chem. Chem. Phys.*, 15(41), 17752(2013). https://doi.org/10.1039/c3cp52908h

Liu, Y., Weng, B., Razal, J. M., Xu, Q., Zhao, C., Hou, Y., Seyedin, S., Jalili, R., Wallace, G. G. and Chen, J., High-Performance Flexible All-Solid-State Supercapacitor from Large Free-Standing Graphene-PEDOT/PSS Films, *Sci. Rep.*, 5(1), 17045(2015). https://doi.org/10.1038/srep17045

Manjakkal, L., Dervin, S. and Dahiya, R., Flexible potentiometric pH sensors for wearable systems, *R. Soc. Chem. Adv*, 10(15), 8594–8617(2020). https://doi.org/10.1039/D0RA00016G

Purkait, T., Singh, G., Kumar, D., Singh, M. and Dey, R. S., High-performance flexible supercapacitors based on electrochemically tailored three-dimensional reduced graphene oxide networks, *Sci. Rep.*, 8(1), 640(2018). https://doi.org/10.1038/s41598-017-18593-3

Qiao, X., Liao, S., You, C. and Chen, R., Phosphorus and Nitrogen Dual Doped and Simultaneously Reduced Graphene Oxide with High Surface Area as Efficient Metal-Free Electrocatalyst for Oxygen Reduction, *Catal.*, 5(2), 981–991(2015). https://doi.org/10.3390/catal5020981

Ratha, S. and Rout, C. S., Supercapacitor Electrodes Based on Layered Tungsten Disulfide-Reduced Graphene Oxide Hybrids Synthesized by a Facile Hydrothermal Method, *Am. Chem. Soc. Appl. Mater. Interfaces*, 5(21), 11427–11433(2013). https://doi.org/10.1021/am403663f

Sambath, K. K., Cherusseri, J. and Thomas, J., Two-Dimensional Mn_3O_4 Nanowalls Grown on Carbon Fibers as Electrodes for Flexible Supercapacitors, *Am. Chem. Soc. Omega*, 4(2), 4472–4480(2019). https://doi.org/10.1021/acsomega.8b03309

Shao, Y., El-Kady, M. F., Sun, J., Li, Y., Zhang, Q., Zhu, M., Wang, H., Dunn, B. and Kaner, R. B., Design and Mechanisms of Asymmetric Supercapacitors, *Chem. Rev.*, 118(18), 9233–9280(2018). https://doi.org/10.1021/acs.chemrev.8b00252

Sharma, M. and Deb, P., WS2 nanosheets with enhanced performances for supercapacitors,. Ranchi, India, *Am. Inst. Phy.*. 020184 (2024). https://doi.org/10.1063/5.0178187

Shen, J., Ji, J., Dong, P., Baines, R., Zhang, Z., Ajayan, P.M., and Ye, M., Novel $FeNi_2S_4$ /TMD-based ternary composites for supercapacitor applications, *J. Mater. Chem. A.*, 4(22), 8844–8850(2016). https://doi.org/10.1039/C6TA03111K

Sun, Y., Wu, Q. and Shi, G., Supercapacitors based on self-assembled graphene organogel, *Phys. Chem. Phys.*, 13(38), 17249(2011). https://doi.org/10.1039/c1cp22409c

Thripuranthaka, M., Kashid, R. V., Sekhar, R. C. and Late, D. J., Temperature dependent Raman spectroscopy of chemically derived few layer MoS2 and WS2 nanosheets, *Appl. Phy. Lett.*, 104(8), 081911(2014). https://doi.org/10.1063/1.4866782

Tu, C. C., Lin, L. Y., Xiao, B. C. and Chen, Y. S., Highly efficient supercapacitor electrode with two-dimensional tungsten disulfide and reduced graphene oxide hybrid nanosheets, *J. Power Sources*, 320, 78–85(2016). https://doi.org/10.1016/j.jpowsour.2016.04.083

Xia, X., Zhang, Y., Chao, D., Xiong, Q., Fan, Z., Tong, X., Tu, J., Zhang, H. and Fan, H. J., Tubular TiC fibre nanostructures as supercapacitor electrode materials with stable cycling life and wide-temperature performance, *Energy Environ. Sci.*, 8(5), 1559–1568(2015). https://doi.org/10.1039/C5EE00339C